博 士 論 文

Identifying bioactive properties of graphene oxide scaffold for bone tissue engineering therapy

（骨組織再生用酸化グラフェンスキャフォールドの生体活性評価）

平成 28 年 3 月申請

北海道大学

大学院歯学研究科口腔医学専攻

西田　絵利香

Identifying bioactive properties of graphene oxide scaffold for bone tissue engineering therapy

Erika NISHIDA, Hirofumi MIYAJI and Masamitsu KAWANAMI

Department of Periodontology and Endodontology, Hokkaido University Graduate School of Dental Medicine, Sapporo, 060-8586, Japan

Correspondence address
Erika NISHIDA
E-mail: erikanishida@den.hokudai.ac.jp

Keywords
Graphene oxide, scaffold, cell ingrowth, biocompatibility, bone tissue engineering

Abstract

Graphene oxide (GO), consisting of a carbon monolayer, has been widely investigated for tissue engineering platforms because of its unique properties. For this study, we fabricated GO-applied scaffold and assessed the physical properties and cellular and tissue behaviors in the scaffold. In addition, a preclinical test was conducted to ascertain whether the GO scaffold promoted bone induction in dog tooth extraction sockets. Results showed that GO application improved the physical strength, enzyme resistance, and adsorption of calcium and proteins. In a cytocompatibility test, GO application was found to increase osteoblastic MC3T3-E1 cell proliferation significantly. In addition, an assessment of rat subcutaneous tissue response showed that implantation of GO scaffold stimulated cellular in-growth behavior, suggesting that the GO scaffold exhibited good biocompatibility. Particularly, the infiltration of ED2- positive (M2) macrophages and blood vessels were prominent in the GO scaffold. In a dog bone-formation test, the GO scaffold implantation enhanced bone formation. New bone formation following GO scaffold implantation was enhanced approximately five-fold compared to that in control. These results suggest that GO provided biocompatibility and bone forming capability for the scaffold. Therefore, the GO scaffold is expected to be available for bone tissue engineering therapy.

The bioactivity of GO scaffold

1. Introduction

Tissue engineering therapy, which is intended to reconstruct tissues lost because of destructive diseases such as inflammation and tumors, requires three major elements: cells, signaling molecules, and scaffolds[1, 2]. Many investigators have developed natural and artificial three-dimensional (3D) scaffolds for tissue engineering of various tissues. The scaffolds provide the field and space for retaining growth and nutrition factors to facilitate the repopulation and differentiation of stem cells[3], blood vessels, and extracellular matrices[4, 5]. Recently, scaffolds in combination with stem cell-seeding and growth factor-application were useful for predictable tissue regeneration[6, 7]. Therefore, refinement of the scaffold specifications for regenerative medicine is expected to be requested for up-regulating bioactive properties including the self-assembly of compound tissues and organs in clinical use. To improve the scaffold therapy efficiency, nano-sized substances have been provided recently for use as regenerative biomaterials. The nanostructured surfaces of biomaterials have greatly increased the surface area to achieve high roughness and wettability[8, 9]. In addition, nanostructures formed on regenerative devices greatly promote biological behaviors such as cell adhesion, migration, proliferation, and differentiation[10–12]. Accordingly, nanotechnology related to tissue engineering therapy is expected to be useful as a contribution to scaffold biologic development and to physiologic improvements.

Carbon-based nano-substrates such as carbon nanotubes (CNTs)[13, 14], carbon nanohorns[15], carbon nanofibers[16] and graphene[17, 18] have been investigated widely for stem cell therapies and tissue engineering platforms because of their unique physical, chemical, and mechanical properties. Graphene oxide (GO), consisting of a two-dimensional honeycomb lattice of a carbon monolayer, is obtained by oxidation and exfoliation of graphite[19]. It exhibits high dispersibility[20] and hydrophilicity[21]. Particularly, the outstanding surface activity of GO, which is most likely caused by many functional groups on its surface, can exert adsorptive capability to drugs[22, 23], growth factors[24] and other biomolecules[25], and can consequently provide important benefits related to tissue engineering therapy. In addition, several in vitro experiments have demonstrated that the use of GO markedly increased the degree of proliferation and differentiation of cultured cells, thereby suggesting that GO possesses good biocompatibility[26-28]. Dinescu et al. reported that the application of GO to the chitosan 3D scaffold stimulated the formation of the interconnected pore structure and enhanced the proliferative activity of attached cells[29]. In addition, Wu et al. demonstrated that β-tricalcium phosphate scaffold modified with GO definitively accelerated the formation of new bone compared to non-modified scaffold in rabbit cranial bones[30]. Therefore, nano-modification using GO might play a major role in providing excellent bioactivity to a regenerative scaffold and might promote subsequent bio-integration between the scaffold and surrounding tissue in bone tissue engineering therapy.

The dosage of nanomaterial application is an important matter related to biocompatibility because high doses of nanomaterials frequently stimulate adverse effects following biomedical application. Huang et al. reported that the application of hydroxyapatite (HA) nanoparticles smaller

than 100 nm diameter with high concentration stimulated the attachment and growth of osteoblastic cells. However, lactate dehydrogenase production of macrophages was also induced[31], thereby suggesting the cytotoxicity of HA nanoparticles. Other studies have shown that nanocarbon materials exhibit toxic effects on cell viability in a time-dependent and dose-dependent manner. Bottini et al. reported that CNTs applied at markedly high concentrations can stimulate human T cell apoptosis[32]. Previously, we created a GO film on a culture dish and assessed the toxic dose effect of GO in association with the viability of cultured osteoblastic MC3T3-E1 cells. Results showed that proliferation and alkaline phosphatase activity of E1 cell decreased in a GO dose-dependent manner. In addition, GO application to a scaffold of type I collagen promoted the mechanical properties of scaffold in a GO dose-dependent manner. However, the cell-ingrowth behavior of GO-applied scaffold in rat connective tissue was inhibited consistently at the loading of GO at higher doses (over 3 wt%)[28]. Furthermore, several investigators have presented similar results by which GO cytotoxicity was exhibited dose-dependently[33, 34]. Therefore, dose setting of GO is expected to play a key role in positive bioeffects and regenerative phenomena for biomedical applications.

To identify the bioactive properties of GO, we created a novel scaffold including low doses of GO, expecting that GO has good bioactivity and anticipating that it is helpful for regenerative scaffold therapy in bone tissue engineering. This study was conducted to assess the cellular and tissue behaviors in relation to a GO scaffold when compared to untreated collagen scaffold in vitro and in vivo. Subsequently, we evaluated, using a preclinical test, whether GO scaffold promotes bone induction in a dog tooth extraction socket, or not.

2. Materials and methods

2.1 Fabrication and GO scaffold

A single-layer GO solution (nano GRAX®; Mitsubishi Gas Chemical, Tokyo, Japan) was prepared in water using Hummers and Offeman's method[35]. The GO monolayer thickness was less than 1 nm. Its average width was approximately 20 μm[36]. Subsequently, GO was dispersed in 1-methyl-2-pyrrolidinone (Wako Pure Chemical, Osaka, Japan) to prepare 0.1 and 1 μg/mL GO dispersion. Then 100 μL of each GO dispersion was injected into 3D collagen sponge-form scaffold (6×6×3 mm, Terudermis®; Olympus Terumo Biomaterials, Tokyo, Japan). After rinsing in ethanol and air-drying, GO scaffolds were obtained for evaluation (Fig. 1A). The collagen scaffold without GO modification was also assessed as control.

2.2 Characterization of GO scaffold

The GO weight attached to collagen scaffolds was measured. The scaffold porosity was calculated according to the following equation: porosity = $100 \times (1-\rho_1/\rho_2)$, where ρ_1 is the bulk density, ρ_2 is the theoretical density of the scaffold. Subsequently, scaffolds were observed using a scanning electron microscope (SEM, S-4000; Hitachi, Tokyo, Japan) at 10 kV. The compressive

strength of scaffolds was measured using a universal testing machine (EZ-S; Shimadzu, Kyoto, Japan) with cross-head loading speed of 0.5 mm/min.

In addition, each scaffold was assessed for enzyme degradation and adsorption of Ca and proteins. Pre-weighed dry scaffolds were immersed for 3 h at 37°C in phosphate buffered saline (PBS) with 1% collagenase type I (Wako Pure Chemical). After ethanol dehydration and air drying, the scaffold weight loss was determined. To detect the Ca adsorption capability, each scaffold was immersed in 0.5 mL fetal bovine serum (FBS; Corning, Mediatech, Kahl/Main, Germany) at 37°C. After rinsing in PBS, the scaffolds were immersed in 0.5 mL acetic acid for 24 h at 37°C. The Ca ion content of the supernatant was assessed using a Calcium E-test WAKO (Wako Pure Chemical). To detect the ability of protein adsorption, each scaffold was injected with 100 μL of sterile distilled water including 50 μg bovine serum albumin (Wako Pure Chemical) or 50 μg lysozyme hydrochloride (from Egg White; Wako Pure Chemical) under a vacuum condition. Subsequently, protein-loaded scaffold was placed in 0.9 mL of deionized distilled water. After stirring well, the protein content of the supernatant was assessed using a total protein kit (Micro Lowry, Peterson's Modification; Sigma-Aldrich, MO). Then adsorption of albumin and lysozyme to the scaffold was calculated.

2.3 Assessment of GO scaffold cytocompatibility

To evaluate GO scaffold cytocompatibility, 5×10^4 mouse osteoblastic MC3T3-E1 cells (RIKEN BioResource Center, Tsukuba, Japan) were seeded on scaffolds and were cultured in humidified 5% CO_2 at 37°C using minimum essential medium (MEM) (alpha-GlutaMAX™-I; Thermo Fisher Scientific, MA) supplemented with 10% FBS (Qualified; Thermo Fisher Scientific) and 1% antibiotics (penicillin/streptomycin; Thermo Fisher Scientific). Cell viability was assessed after 1, 3, 5, and 7 days of culture using a WST-8; cell counting kit-8 (CCK-8; Dojindo, Kumamoto, Japan). The optical density was measured using a microplate reader with absorbance of 450 nm.

After 1 day of culture, some samples were fixed in 2.5% glutaraldehyde in 0.1 M sodium cacodylate buffer (pH 7.4) for 30 min. Then they were routinely processed and analyzed using SEM. Some samples cultured for 7 days were embedded in paraffin and the sections were stained with hematoxylin–eosin (HE).

2.4 Assessment of rat subcutaneous tissue response to GO scaffold

The experimental protocol followed the institutional animal use and care regulations of Hokkaido University (Animal Research Committee of Hokkaido University, Approval No. 13-76). Eighteen 10-week-old male Wistar rats weighing 190–210 g were given general anesthesia by intraperitoneal injection of sodium pentobarbital (Somnopenthyl; Kyoritsu Seiyaku, Tokyo, Japan) and local injection of 2% lidocaine hydrochloride (Xylocaine Cartridge for Dental Use; Dentsply Sankin K.K., Tokyo, Japan). After a skin incision was made in the back, each scaffold was implanted into the subcutaneous tissue. Skin flaps were sutured (Softretch 4-0; GC, Tokyo, Japan) and

tetracycline hydrochloride ointment (Achromycin Ointment; POLA Pharma, Tokyo, Japan) was applied there.

To assess the scaffold DNA contents, several specimens at 10 and 35 days post-surgery were freeze-dried. Following pulverization, 0.5 mL of 2 M NaCl and 0.05 M phosphate buffer (pH 7.4) were added to each scaffold. After centrifugation, DNA contents of infiltrated cells were examined using a DNA quantification kit (Primary Cell, Sapporo, Japan) and a fluorescence spectrophotometer (F-3000; Hitachi) at the respective excitation and emission wavelengths of 356 nm and 458 nm.

For histological observation, 6 samples were collected at 10 days were fixed in 10% buffered formalin for 24 h, embedded in paraffin. The sections were stained with HE and tissue ingrowth area was measured using software (Image J 1.41; National Institutes of Health, Bethesda, MD). In addition, the foreign body giant cells were counted in three area (0.12 mm^2 per unit) at the periphey of scaffold selected under a light microscope. These evaluations were assessed using three stained sections: one from the center of the excised tissue sample, and one from tissue 1 mm to either side of the center.

2.5 Immunohistochemical assessment of implanted GO scaffold

Anesthetized rats were perfused with 4% formaldehyde in 0.1 M phosphate buffer, pH 7.4. Tissues were removed, immersed in the same fixative for an additional 24 h and quickly frozen in liquid nitrogen. After pretreatment with 0.3% Triton X-100 and normal donkey serum, the frozen sections were incubated overnight with the following primary antibodies : mouse anti-CD68 (ED-1) (1:100 in dilution; Bio-Rad, CA), mouse anti-CD163 (ED-2) (1:100 in dilution; Bio-Rad), mouse anti-prolyl-4-hydroxylase beta (P4HB) (1:1600 in dilution, clone6-9H6; Acris Antibodies, CA) and mouse anti-α-smooth muscle actin (ASMA) (1:1600 in dilution, clone 1A4; Sigma-Aldrich). Then the section were incubated with Cy3-labeled anti-mouse IgG (Jackson ImmunoResearch, PA). Nuclear staining was performed with short incubation (TOTO3; Thermo Fisher Scientific). The stained sections were observed under a confocal laser scanning microscope (Fluoview; Olympus). To detect granulocytes, the sections were incubated in 0.01M Tris-HCl buffer (pH 7.6) containing 0.01% 3,3'-diaminobenzidine and 0.001% H_2O_2. The sections incubated with normal mouse serum instead of respective primary antibody were used as negative control.

2.6 Implantation of GO scaffold to extraction sockets of dogs

4 female beagle dogs, aged 10 months and weighing approximately 9–10 kg, were anesthetized with medetomidine hydrochloride (Domitor; Nippon Zenyaku Kogyo, Fukushima, Japan) and butorphanol tartrate (Vetorphale; Meiji Seika Pharma, Tokyo, Japan), in addition to local anesthesia with lidocaine hydrochloride (Approval number 8-255). Following extraction of maxillar third premolars, scaffold applied with 1 μg/mL GO was embedded into the sockets, which were then sutured. At 2 weeks, the animals were euthanized, and the tissue blocks were fixed in 10% buffered formalin after decalcification in 10% formic-citric acid, serial paraffin sections along the mesio-distal

plane were stained with Masson's trichrome (MT). Histomorphometric measurements of the rate of bone formation: the percentage of the newly formed bone area to the total extraction socket area; were performed on the center of the excised tissue sample using a software package. Radiographic images of extraction sockets were taken immediately following surgery and at 2 weeks after scaffold implantation.

2.7 Statistical analysis

Statistical analysis was performed using a Student-*t* test or Scheffé test on each measurement (IBM SPSS 11.0; IBM SPSS Japan, Tokyo, Japan). *P*-values <0.05 were inferred as statistically significant.

3. Results

3.1 Characterization of GO scaffold

In SEM images, the GO scaffold rarely showed striations of collagen fibers that were readily visible on the un-treated collagen scaffold, even on the central region of the scaffold (Figs. 1B, 1C). In SEM images of 1 μg/mL GO scaffold, we frequently found a wrinkled structure of GO without large aggregate formation (Fig. 1D). Actually, the GO scaffold possessed an interconnected structure resembling that of the control (Fig. 1E). The GO-applied scaffold porosity was equivalent to that of the control (Table 1).

The compressive strength of 1 μg/mL GO scaffold was approximately 1.7-fold greater than that of the control. The difference was statistically significant. The strength of 0.1 μg/mL GO scaffold was 1.3-fold greater than that of the control (Fig. 2A). A degradation test showed that application of GO to the scaffolds increased its resistance to enzymatic degradation. The decrement in content in 1 μg/mL GO scaffold was 85.5%, which was significantly less than that of the control (Fig. 2B). The amount of Ca ion adsorption of scaffold was promoted by GO application; the scaffold applied with 1 μg/mL GO was approximately 1.2-fold greater than that of the control (Fig. 2C). Protein adsorption tests showed that GO scaffold exhibited considerable amounts of albumin and lysozyme adsorption. Adsorption percentages of albumin and lysozyme of 1 μg/mL GO scaffold were, respectively, 88% and 40% (Fig. 2D).

3.2 Cytocompatibility of GO scaffold

After MC3T3-E1 cell seeding, cell infiltration was clearly demonstrated on the GO-applied scaffold (Figs. 3A–3C). The SEM images show cell spreading with cell process elongation occurring on the GO-applied collagen fibers (Fig. 3D). WST-8 assessment showed that MC3T3-E1 cell proliferation on the scaffold was stimulated significantly and dose-dependently by GO application. At 7 days, cell proliferation of 1 μg/mL GO scaffold was 1.6-fold greater than that of control (Fig. 3E).

The bioactivity of GO scaffold

3.3 Rat subcutaneous tissue response to GO scaffold

Histological specimens of control (Figs. 4A–4C) and 0.1 μg/mL GO scaffold (Figs. 4D–4F) revealed that the implanted scaffold appeared to be physically compressed in the connective tissue, and that the cell-ingrowth into the scaffold was limited. In contrast, the cell ingrowth, containing fibroblast-like cells, giant cells, and blood vessel-like structures, was remarkable in the 1 μg/mL GO scaffold (Figs. 4G–4I) when compared to 0.1 μg/mL GO scaffold and control. The number of foreign body giant cells, tissue ingrowth area and DNA contents of 1 μg/mL GO scaffold were respectively about 3.0-, 2.5- and 1.4-fold greater than those of the control (Figs. 4J–4L).

3.4 Immunohistochemical investigation of GO scaffold

Specimens of GO-applied scaffold obtained at 10 days after implantation revealed that macrophages expressing ED-1 and ED-2 and fibroblasts expressing P4HB were found frequently in the scaffold (Figs. 5A–5C). Vascular structures formed by ASMA-positive smooth muscle cells were remarkable in 1 μg/mL GO scaffold, especially at the scaffold periphery (Fig. 5D). However, control specimens only slightly exhibited cell ingrowth behavior (Figs. 5E–5H).

In specimens of 1 μg/mL GO scaffold at 35 days, ED1-positive macrophages were decreased and ED2-positive macrophages were abundant when compared to specimens observed at 10 days (Figs. 5I, 5J). The P4HB-positive cells and blood vessels became thicker (Figs. 5K, 5L). In control specimens, cell ingrowth behavior at 35 days resembled that in 10 day specimens (Figs. 5M–5P).

Peroxidase-positive granulocytes were detected to a slight degree around 1 μg/mL GO scaffold at 10 and 35 days post-surgery (Figs. 6A, 6C), in contrast to control specimens, in which granulocytes were rarely observed (Figs. 6B, 6D).

3.5 Implantation of GO scaffold to extraction sockets in dogs

The postoperative healing process exhibited the progress well in all four dogs examined (Figs. 7A, 7D). The sockets applied with GO scaffold and collagen scaffold showed increased radiopacity at 2 weeks post-surgery (Figs. 7B, 7C, 7E, 7F). Histological specimens revealed that GO scaffold application promoted the formation of new bone in the socket (Figs. 8A–8C). GO aggregation was frequently found in newly formed bone, bone marrow, and connective tissue (Figs. 8B, 8C). New bone formation was limited in the implantation of control scaffold, where most of the socket was filled with connective tissue (Figs. 8D, 8E). The rate of new bone formation in GO-applied specimens increased significantly when compared with control. Mean values for new bone of GO scaffold were approximately five-fold greater than in control (Fig. 8F).

4. Discussion

This study demonstrated that surface modification by GO can provide remarkable bioactivities to 3D scaffold made by collagen. Particularly in vitro cell proliferation was strongly up-regulated, as were in vivo cell and blood vessel ingrowth effects. Ordinarily, the scaffold for tissue engineering

requires exhibition of biocompatible morphology and properties, as well as porous structure and physical strength[37]. In addition, the surface morphology of the interface between cells and biomaterials strongly affects the cell behavior in terms of cell migration, proliferation, and differentiation[38, 39]. The application of nanoparticle-modified structure might increase the surface area and subsequent signaling molecule adsorption, thereby improving cell behaviors[10–12, 40]. The present SEM observation in 1 μg/mL GO scaffold demonstrated that wrinkling structures covered by GO sheets were formed frequently on the collagen strut of the scaffold. The GO sheet possesses many functional groups including hydroxyl (OH), epoxy (C–O–C), and carboxyl (COOH) species on its surface. Therefore, GO can adsorb some biomolecules to improve their chemical and biological properties[41]. In fact, GO-applied scaffold was able to adsorb both acid protein (albumin) and basic protein (lysozyme) in the protein adsorption test. Therefore, various biological molecules supplied by FBS would be retained on GO surface and provide cytocompatibility effects for MC3T3-E1 cell infiltration and proliferation in the scaffold. Ryoo et al. reported that focal adhesion of NIH-3T3 fibroblastic cells on the GO substrate surface was promoted and that an attachment protein, vinculin, was expressed abundantly on the cells by the GO. They concluded that the GO surface is biocompatible[42].

Actually, GO application stimulated the cell and tissue ingrowth in rat subcutaneous tissues. Macrophages are known to secrete various cytokines that stimulate the formation of granulation tissue, and which frequently reconstruct bone tissue[43]. Immunohistochemical assessment of 1 μg/mL GO scaffolds at 10 and 35 days after implantation revealed enhanced infiltration of macrophages expressing ED-1, fibroblasts expressing P4HB and neutrophils in the scaffold. That result suggests that GO induces scaffold degradation, reflecting phagocytosis by macrophages, and that it causes the subsequent production of extracellular matrix such as collagen. Furthermore, the 1 μg/mL GO scaffold actively caused formation of blood vessels including arterioles with ASMA-positive smooth muscle cells. Consequently, GO application is expected to stimulate angiogenesis to provide oxygen and nutrition supply effectively for tissue remodeling. Lucas et al. reported that activated macrophages controlled the natural sequence of repair event in wound healing[44]. Activated macrophages are classified into activated macrophages (M1 macrophage) and wound healing macrophages (M2 macrophage). The latter are associated with immunosuppression and with tissue repair and remodeling, playing critical roles in the resolution of inflammatory responses[45, 46]. In this study, ED2-positive M2 macrophages, were remarkable in 1 μg/mL GO scaffold at 10 and 35 days post-surgery, in contrast to the control, which scarcely contained ED2-positive macrophages, suggesting that GO application to the scaffold enhances tissue repair via macrophage recruitment.

The examinations of physical properties of the scaffold presented herein revealed that GO application reinforced compressive strength and collagenase resistance, by the wrapping of scaffold collagen fibers with GO nanofilms and by the deep infiltration of GO into collagen scaffold. The GO coating layer has been shown to enhance the collagen scaffold stability because of attractive force by its nanoscale distance[47]. In bone regenerative therapy, the mechanical stiffness of scaffold was able

to play an important role in maintaining a tissue-reconstructive inner space for osteogenic cells such as osteoblasts[48]. Although regenerative scaffolds should be designed to provide a highly porous structure for stimulating tissue ingrowth, higher porosity generally causes lower mechanical strength[49]. In the present study, the GO scaffold porosity was equivalent to that of the control. An SEM image of 1 μg/mL GO exhibited an interconnected porous structure with high porosity. Therefore, regenerative cells were able to infiltrate into the scaffold. In histological findings of rat subcutaneous tissue, 1 μg/mL GO scaffold maintained space for tissue reconstruction. Moreover, the 0.1 μg/mL GO scaffold was compressed as in the control. Although a previous study revealed that the high-dose application of GO (10 μg/mL) to the scaffold strongly promoted the scaffold mechanical strength, it also inhibited cell infiltration into the scaffold[28]. Wang et al. reported that GO exhibited marked cytotoxicity that included decreasing cell adhesion and induction of cell apoptosis[33]. Accordingly, we speculate that GO application at low doses (1 μg/mL) eliminated adverse effects and stimulated tissue response as a catalytic effect.

Bone formation assessment of dog extraction sockets revealed that providing a GO scaffold promoted bone induction significantly, suggesting that GO scaffold had positive effects on osteoblastic cell responses in addition to improving their physical properties. Based on rat subcutaneous experiments, GO scaffold conceivably guided cells of various types related to bone induction from tissue surrounding the extraction socket. Subsequently, the production of extracellular matrix and circulation induced by angiogenesis might occur in the GO scaffold. Early regenerative tissue accumulation might precede epithelial tissue invasion into the socket. An earlier study revealed that GO application enhanced the bioactivities of bone marrow stromal cells such as proliferation, alkaline phosphatase activity, and expression of Wnt signaling pathway associated with osteogenic differentiation[30]. In addition, many functional groups on the GO surface are well-suited to interaction with cations and anions, thereby enhancing Ca adsorption[41, 50, 51]. We speculate that the Ca adsorption of GO scaffold was enhanced by graphite intercalation, i.e., insertion of Ca between GO nanolayers. Results show that Ca ion stimulated the expression of osseous markers in osteoblastic cells, stimulated alkaline phosphatase activity, and adjusted the in vivo environment for bone generation[52, 53]. As demonstrated in this study, Ca accumulation on the surface of GO scaffold might provide a favorable environment for bone tissue formation.

5. Conclusion

Effects of GO application to the 3D collagen scaffold were variously examined in vitro and in vivo. GO application promoted collagen scaffold physical properties such as compressive strength, enzyme resistance, and adsorption of Ca and proteins. Osteoblastic MC3T3-E1 cell proliferation was remarkable on the GO-applied scaffold. GO application also stimulated biological effects. Particularly, scaffold applied with 1 μg/mL GO remarkably exerted cell and tissue-ingrowth behavior as well as angiogenesis in rat subcutaneous tissues. In the extraction sockets of dogs, GO scaffold exhibited approximately five-fold increased bone formation when compared to the collagen scaffold.

The bioactivity of GO scaffold

These results suggest that GO provided biocompatibility and high bone-forming capability for the scaffold. Therefore, GO scaffold is expected to be useful and beneficial for bone tissue engineering therapy.

Acknowledgments

The authors thank Mitsubishi Gas Chemical Co. Inc. for providing nanoGRAX® and Olympus Terumo Biomaterials Corp. for providing collagen scaffolds. This work was supported by JPSP KAKENHI Grant Numbers 22791916 and 25463210. The authors report that they have no conflict of interest related to this study.

The bioactivity of GO scaffold

References

1) Yang S, Leong KF, Du Z, Chua CK: The design of scaffolds for use in tissue engineering. Part I. Traditional factors. Tissue Eng 7 : 679-689, 2001.

2) Chen FM, Jin Y: Periodontal tissue engineering and regeneration: current approaches and expanding opportunities. Tissue Eng Part B Rev 16 : 219-255, 2010.

3) Li WJ, Tuli R, Huang X, Laquerriere P, Tuan RS: Multilineage differentiation of human mesenchymal stem cells in a three-dimensional nanofibrous scaffold. Biomaterials 26 : 5158-5166, 2005.

4) Hutmacher DW: Scaffolds in tissue engineering bone and cartilage. Biomaterials 21 : 2529-2543, 2000.

5) Lutolf MP, Hubbell JA: Synthetic biomaterials as instructive extracellular microenvironments for morphogenesis in tissue engineering. Nat Biotechnol 23 : 47-55, 2005.

6) Teng YD, Lavik EB, Qu X, Park KI, Ourednik J, Zurakowski D, Langer R, Snyder EY: Functional recovery following traumatic spinal cord injury mediated by a unique polymer scaffold seeded with neural stem cells. Proc Natl Acad Sci U S A 99 : 3024-3029, 2002.

7) Kim S, Kim SS, Lee SH, Eun Ahn S, Gwak SJ, Song JH, Kim BS, Chung HM: In vivo bone formation from human embryonic stem cell-derived osteogenic cells in poly(D,L-lactic-co-glycolic acid)/hydroxyapatite composite scaffolds. Biomaterials 29 : 1043-1053, 2008.

8) Zhou W, Zhong X, Wu X, Yuan L, Zhao Z, Wang H, Xia Y, Feng Y, He J, Chen W: The effect of surface roughness and wettability of nanostructured TiO2 film on TCA-8113 epithelial-like cells. Surf Coat Technol 200 : 6155-6160, 2006.

9) Rosales-Leal JI, Rodríguez-Valverde MA, Mazzaglia G, Ramón-Torregrosa PJ, Díaz-Rodríguez L, García-Martínez O, Vallecillo-Capilla M, Ruiz C, Cabrerizo-Vílchez MA: Effect of roughness, wettability and morphology of engineered titanium surfaces on osteoblast-like cell adhesion. Colloid Surf A 365 : 222-229, 2010.

10) Thapa A, Miller DC, Webster TJ, Haberstroh KM: Nano-structured polymers enhance bladder smooth muscle cell function. Biomaterials 24 : 2915-2926, 2003.

11) Huang HH, Ho CT, Lee TH, Lee TL, Liao KK, Chen FL: Effect of surface roughness of ground titanium on initial cell adhesion. Biomol Eng 21 : 93-97, 2004.

12) Zhang L, Ramsaywack S, Fenniri H, Webster TJ: Enhanced Osteoblast Adhesion on Self-Assembled Nanostructured Hydrogel Scaffolds. Tissue Eng Part A 14 : 1353-1364, 2008.

13) Usui Y, Aoki K, Narita N, Murakami N, Nakamura I, Nakamura K, Ishigaki N, Yamazaki H, Horiuchi H, Kato H, Taruta S, Kim YA, Endo M, Saito N: Carbon nanotubes with high bone-tissue compatibility and bone-formation acceleration effects. Small 4: 240-246. 2008.

14) Han ZJ, Rider AE, Ishaq M, Kumar S, Kondyurin A, Bilek MMM, Levchenko I, Ostrikov K: Carbon nanostructures for hard tissue engineering. RSC Adv 3 : 11058-11072, 2013.

15) Kasai T, Matsumura S, Iizuka T, Shiba K, Kanamori T, Yudasaka M, Iijima S, Yokoyama A: Carbon nanohorns accelerate bone regeneration in rat calvarial bone defect. Nanotechnology 22 : 065102, 2011.
16) Elias KL, Price RL, Webster TJ: Enhanced functions of osteoblasts on nanometer diameter carbon fibers. Biomaterials 23 : 3279-3287, 2002.
17) Chen GY, Pang DWP, Hwang SM, Tuan HY, Hu YC: A graphene-based platform for induced pluripotent stem cells culture and differentiation. Biomaterials 33 : 418-427, 2012.
18) Tang M, Song Q, Li N, Jiang Z, Huang R, Cheng G: Enhancement of electrical signaling in neural networks on graphene films. Biomaterials 34 : 6402-6411, 2013.
19) Dikin DA, Stankovich S, Zimney EJ, Piner RD, Dommett GH, Evmenenko G, Nguyen ST, Ruoff RS: Preparation and characterization of graphene oxide paper. Nature 448 : 457-460, 2007.
20) Dreyer DR, Park S, Bielawski CW, Ruoff RS: The chemistry of graphene oxide. Chem Soc Rev 39 : 228-240, 2010.
21) Marcano DC, Kosynkin DV, Berlin JM, Sinitskii A, Sun Z, Slesarev A, Alemany LB, Lu W, Tour JM: Improved synthesis of graphene oxide. ACS Nano 4 : 4806-4814, 2010.
22) Sun X, Liu Z, Welsher K, Robinson JT, Goodwin A, Zaric S, Dai H: Nano-Graphene Oxide for Cellular Imaging and Drug Delivery. Nano Res 1 : 203-212, 2008.
23) Sayyar S, Murray E, Thompson BC, Gambhir S, Officer DL, GG Wallace: Covalently linked biocompatible graphene/polycaprolactone composites for tissue engineering. Carbon 52 : 296-304, 2013.
24) La WG , Park S , Yoon HH, Jeong GJ, Lee TJ, Bhang SH, Han JY, Char K, Kim BS: Delivery of a therapeutic protein for bone regeneration from a substrate coated with graphene oxide. Small 9 : 4051-4060, 2013.
25) Qin W, Li X, Bian WW, Fan XJ, Qi JY: Density functional theory calculations and molecular dynamics simulations of the adsorption of biomolecules on graphene surfaces. Biomaterials 31 : 1007-1016, 2010.
26) Goenka S, Sant V, Sant S: Graphene-based nanomaterials for drug delivery and tissue engineering. J Control Release 143 : 75-88, 2014.
27) Lee WC, Lim CH, Tang LA, Wang Y, Lim CT, Loh KP: Origin of enhanced stem cell growth and differentiation on graphene and graphene oxide. ACS Nano 5 : 7334-41, 2011.
28) Nishida E, Miyaji H, Takita H, Kanayama I, Tsuji M, Akasaka T, Sugaya T, Sakagami R, Kawanami M: Graphene oxide coating facilitates the bioactivity of scaffold material for tissue engineering. Jpn J Appl Phys 53 : 06JD04, 2014.
29) Dinescu S, Ionita M, Pandele AM, Galateanu B, Iovu H, Ardelean A, Costache M, Hermenean A: In vitro cytocompatibility evaluation of chitosan/graphene oxide 3D scaffold composites designed for bone tissue engineering. Biomed Mater Eng 24 : 2249-2256, 2014.

30) Wu C, Xia L, Han P, Xu M, Fang B, Wang J, Chang J, Xiao Y: Graphene-oxide-modified β-tricalcium phosphate bioceramics stimulate in vitro and in vivo osteogenesis. Carbon 93, 116-129, 2015.
31) Huang J, Best SM, Bonfield W, Brooks RA, Rushton N, Jayasinghe SN, Edirisinghe MJ: In vitro assessment of the biological response to nano-sized hydroxyapatite. J Mater Sci Mater Med 15 : 441-445, 2004.
32) Bottini M, Bruckner S, Nika K, Bottini N, Bellucci S, Magrini A, Bergamaschi A, Mustelin T: Multi-walled carbon nanotubes induce T lymphocyte apoptosis. Toxicol Lett 160 : 121-126, 2006.
33) Wang K, Ruan J, Song H, Zhang J, Wo Y, Guo S, Cui D: Biocompatibility of graphene oxide. Nanoscale Res Lett 6 : 8, 2011.
34) Liao KH, Lin YS, Macosko CW, Haynes CL: Cytotoxicity of graphene oxide and graphene in human erythrocytes and skin fibroblasts. ACS Appl Mater Interfaces 3 : 2607-2615, 2011.
35) Hummers Jr WS, Offeman RE: Preparation of graphitic oxide. J Am Chem Soc 80 : 1339, 1958.
36) Hirata M, Gotou T, Horiuchi S, Fujiwara M, Ohba M: Thin-film particles of graphite oxide 1:: High-yield synthesis and flexibility of the particles. Carbon 42 : 2929-2937, 2004.
37) Salgado AJ, Coutinho OP, Reis RL. Bone tissue engineering: state of the art and future trends. Macromol Biosci 4 : 743-765, 2004.
38) Ibara A, Miyaji H, Fugetsu B, Nishida E, Takita H, Tanaka S, Sugaya T, Kawanami M: Osteoconductivity and biodegradability of collagen scaffold coated with nano-β-TCP and fibroblast growth factor 2. J Nanomater : 639502, 2013.
39) Yoshida T, Miyaji H, Otani K, Inoue K, Nakane K, Nishimura H, Ibara A, Shimada A, Ogawa K, Nishida E, Sugaya T, Sun L, Fugetsu B, Kawanami M: Bone augmentation using a highly porous PLGA/β-TCP scaffold containing fibroblast growth factor-2. J Periodont Res 50 : 265-273, 2015.
40) Miyaji H, Sugaya T, Ibe K, Ishizuka R, Tokunaga K, Kawanami M: Root surface conditioning with bone morphogenetic protein-2 facilitates cementum-like tissue deposition in beagle dogs. J Periodontal Res 45 : 658-663, 2010.
41) Li M, Wang Y, Liu Q, Li Q, Cheng Y, Zheng Y, Xi T, Wei S: In situ synthesis and biocompatibility of nano hydroxyapatite on pristine and chitosan functionalized graphene oxide. J Mater Chem B 1 : 475-484, 2013.
42) Ryoo SR, Kim YK, Kim MH, Min DH: Behaviors of NIH-3T3 fibroblasts on graphene/carbon nanotubes: proliferation, focal adhesion, and gene transfection studies. ACS Nano 4 : 6587-6598, 2010.
43) Kim YH, Furuya H, Tabata Y: Enhancement of bone regeneration by dual release of a macrophage recruitment agent and platelet-rich plasma from gelatin hydrogels. Biomaterials 35 : 214-224, 2014.
44) Lucas T, Waisman A, Ranjan R, Roes J, Krieg T, Müller W, Roers A, Eming SA: Differential roles of macrophages in diverse phases of skin repair. J Immunol 184 : 3964-3677, 2010.

45) Mantovani A, Biswas SK, Galdiero MR, Sica A, Locati M: Macrophage plasticity and polarization in tissue repair and remodeling. J Pathol 229 : 176-185, 2013.
46) Ito T, Kaneko T, Yamanaka Y, Shigetani Y, Yoshiba K, Okiji T: M2 macrophages participate in the biological tissue healing reaction to mineral trioxide aggregate. J Endod 40 : 379-383, 2014.
47) Kanayama I, Miyaji H, Takita H, Nishida E, Tsuji M, Fugetsu B, Sun L, Inoue K, Ibara A, Akasaka T, Sugaya T, Kawanami M: Comparative study of bioactivity of collagen scaffolds coated with graphene oxide and reduced graphene oxide. Int J Nanomedicine 9 : 3363-3373, 2014.
48) Liu X, Smith LA, Hu J, Ma PX: Biomimetic nanofibrous gelatin/apatite composite scaffolds for bone tissue engineering. Biomaterials 30 : 2252-2258, 2009.
49) Karageorgiou V, Kaplan D: Porosity of 3D biomaterial scaffolds and osteogenesis. Biomaterials 26 : 5474-5491, 2005.
50) Depan D, Girase B, Shah JS, Misra RDK: Structure–process–property relationship of the polar graphene oxide-mediated cellular response and stimulated growth of osteoblasts on hybrid chitosan network structure nanocomposite scaffolds. Acta Biomater 7 : 3432-3445, 2011.
51) Girase B, Shah JS, Misra RDK: Cellular mechanics of modulated osteoblasts functions in graphene oxide reinforced elastomers. Adv Eng Mater 14 : B101-111, 2012.
52) Sugimoto T, Kanatani M, Kano J, Kaji H, Tsukamoto T, Yamaguchi T, Fukase M, Chihara K: Effects of high calcium concentration on the functions and interactions of osteoblastic cells and monocytes and on the formation of osteoclast-like cells. J Bone Miner Res 8 : 1445-1452, 1993.
53) Lü LX, Zhang XF, Wang YY, Ortiz L, Mao X, Jiang ZL, Xiao ZD, Huang NP: Effects of hydroxyapatite-containing composite nanofibers on osteogenesis of mesenchymal stem cells in vitro and bone regeneration in vivo. ACS Appl Mater Interfaces 5 : 319-330, 2013.

The bioactivity of GO scaffold

Table 1. Structural parameters of the scaffold (N = 5, mean ± SD)

	control	0.1 μg/mL GO scaffold	1 μg/mL GO scaffold
GO weight (wt %)	--	1.83 ± 0.57	2.22 ± 0.71
Porosity (%)	97.63 ± 0.05	97.60 ± 0.08	97.60 ± 0.06

The bioactivity of GO scaffold

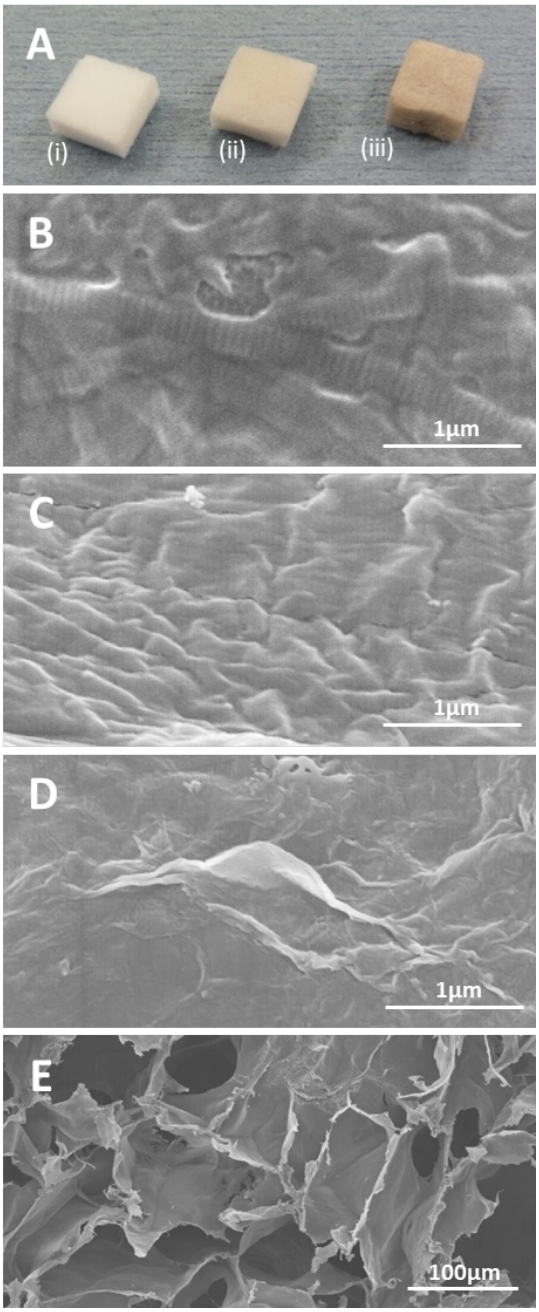

Figure 1

(A) Photographs of collagen scaffold (i), 0.1 µg/mL GO scaffold (ii), and 1 µg/mL GO scaffold (iii). SEM images of collagen scaffold (b), 0.1 µg/mL GO scaffold (C) and 1 µg/mL GO scaffold (D, E). (D) The wrinkled structure of GO was observed on collagen fibers. (E) GO scaffold possessed interconnected structure.

The bioactivity of GO scaffold

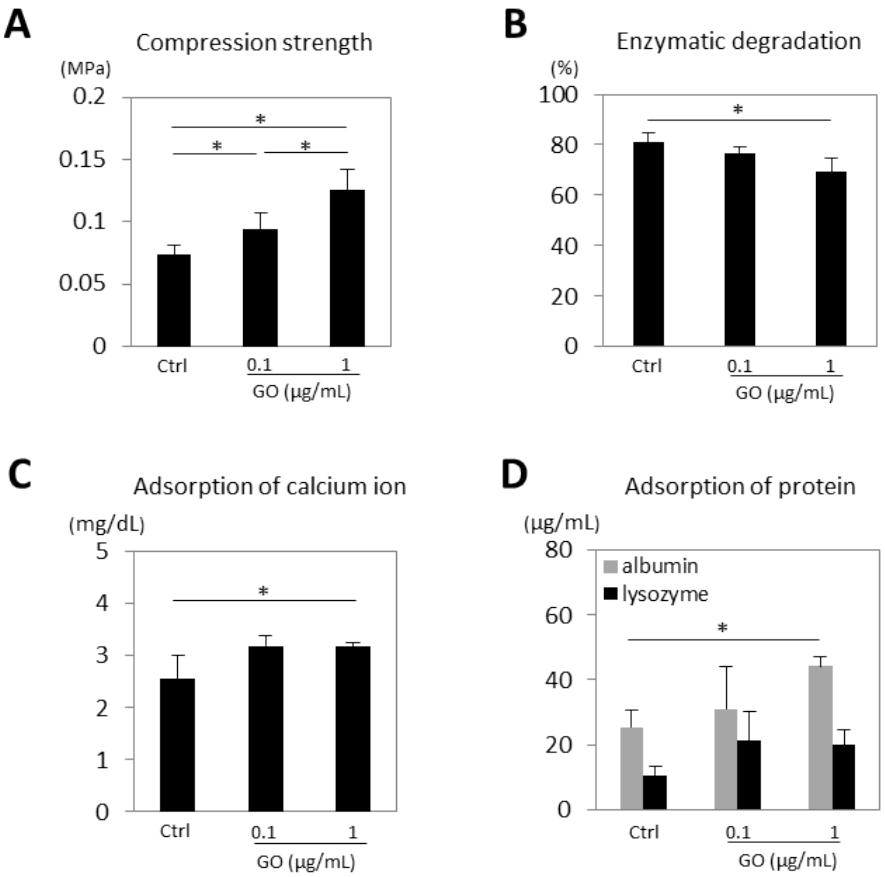

Figure 2

(A–D) In vitro assessment of each scaffold (N = 6, mean ± SD). P<0.05, a vs. control, b vs. 0.1 μg/mL GO scaffold.

The bioactivity of GO scaffold

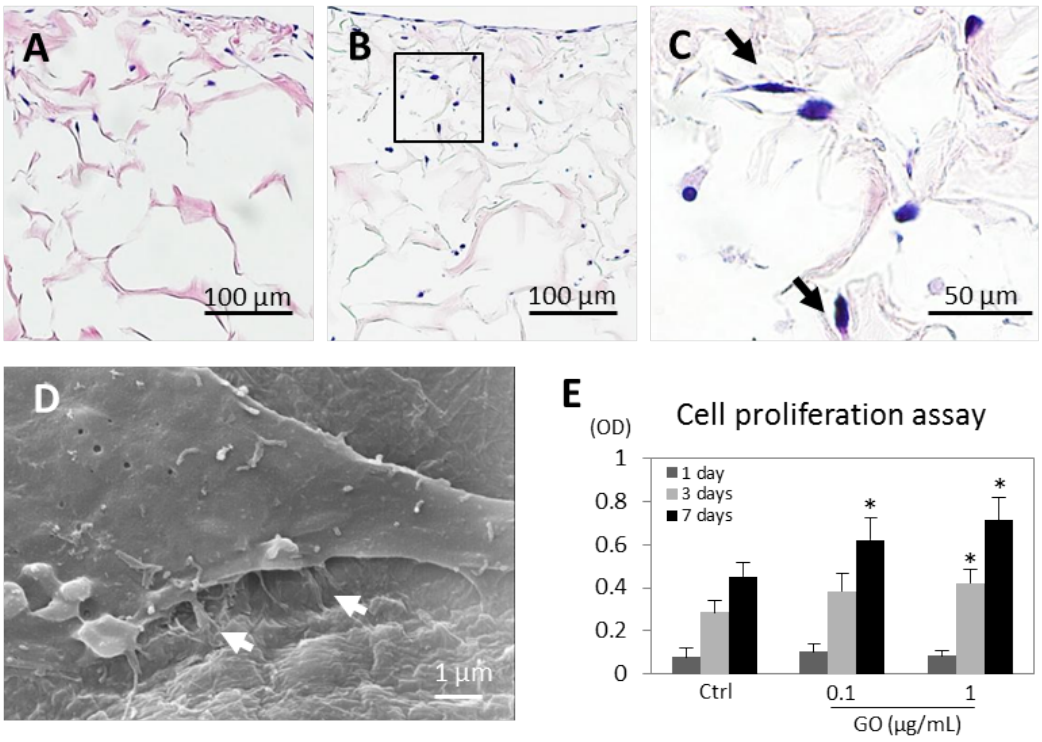

Figure 3

Microscopic images of control (A) and 1 µg/mL GO scaffold (B) with MC3T3-E1 cells after 7 days incubation. (C) Higher magnification of the framed area in B. Cultured cells (arrows) were frequently detected in the GO scaffold. (D) SEM image of 1 µg/mL GO scaffold with MC3T3-E1 cells after 1 day incubation. Cell spreading with fine processes elongation (white arrows) was observed. (E) WST-8 assay ($N = 6$, mean ± SD). *: $P<0.05$, vs. control.

The bioactivity of GO scaffold

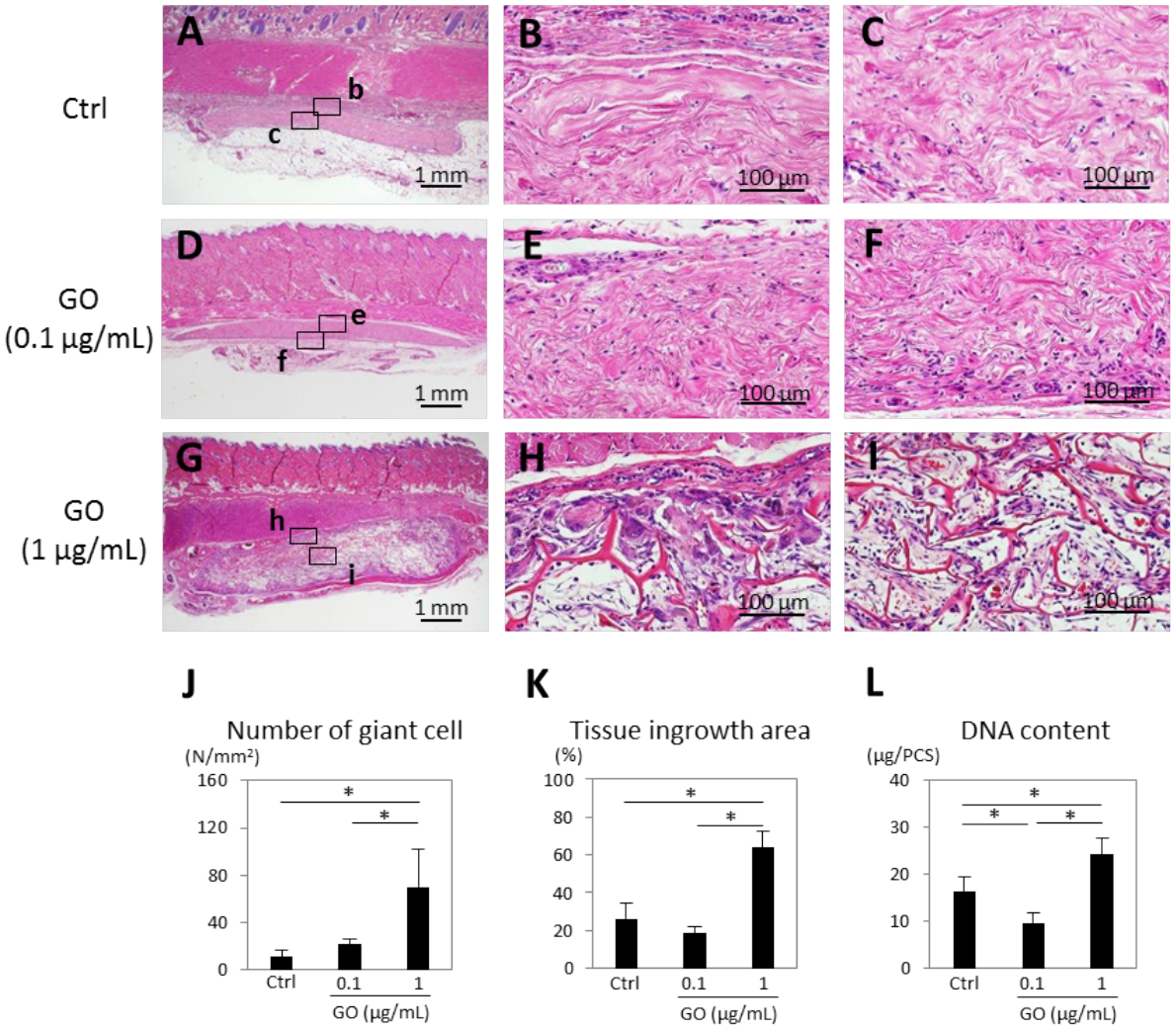

Figure 4

Histological findings for control (A–C), 0.1 µg/mL GO scaffold (D–F) and 1µg/mL GO scaffold (G–L) in rat subcutaneous tissue at 10 days. Rectangles (b, c, e, f, h and i) in Figs. A, D and G are enlarged in Figs. B, C, E, F, H and I, respectively. Cell and tissue ingrowth behavior was remarkable in 1 µg/mL GO scaffold. Hematoxylin–eosin staining. (J–L) In vivo assessment of each scaffold for number of giant cells, tissue ingrowth area, and DNA content ($N = 6$, mean ± SD). *: $P<0.05$.

The bioactivity of GO scaffold

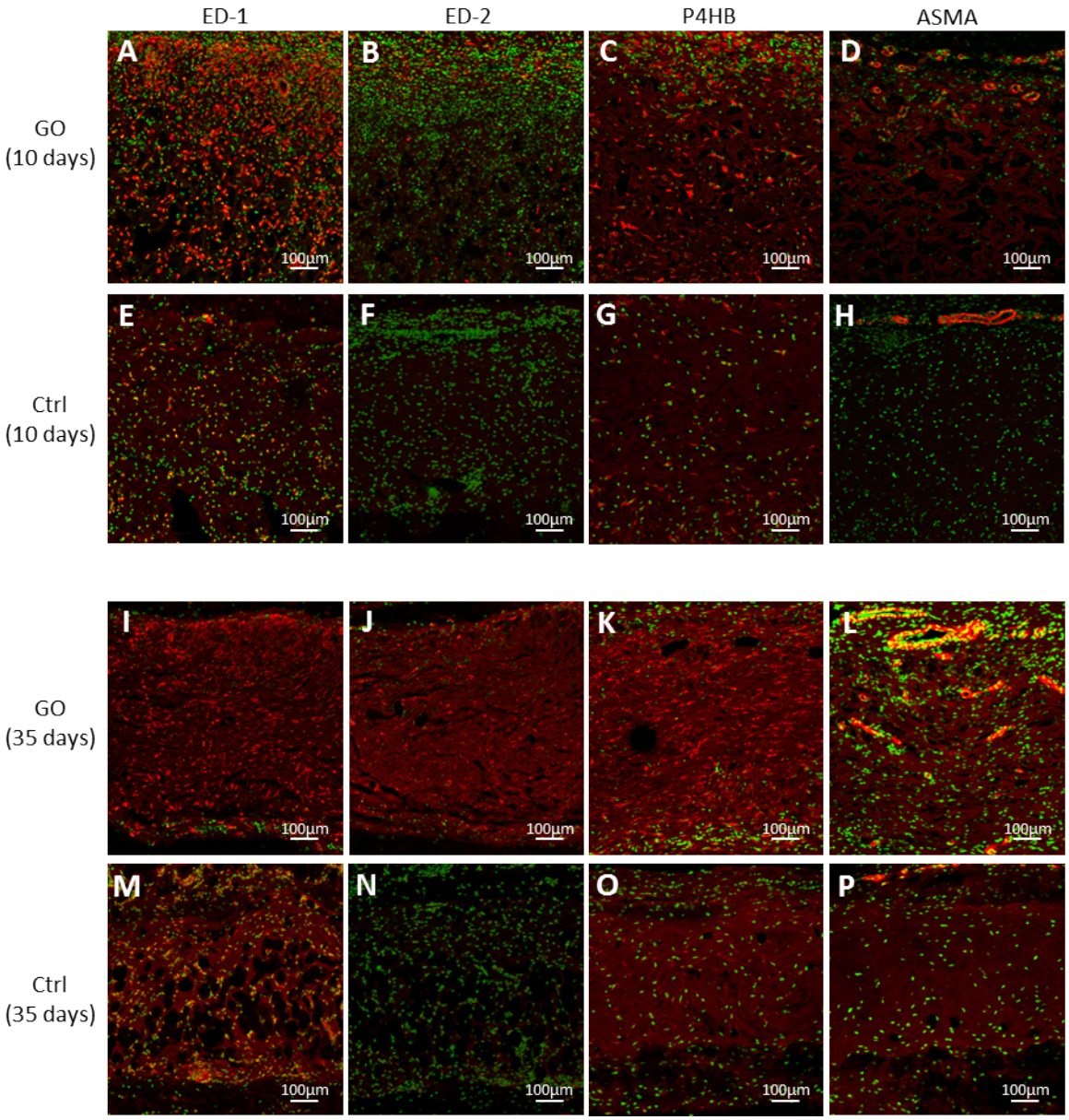

Figure 5

Immunofluorescence micrographs of macrophages, fibroblasts, and blood vessel cryostat sections stained (in red) with mouse anti-CD68 (ED-1) (A, E, I, M), mouse anti-CD163 (ED-2) (B, F, J, N), mouse anti-prolyl-4-hydroxylase beta (P4HB) (C, G, K, O) and mouse anti-α-smooth muscle actin (ASMA) (D, H, I, P) for 1 µg/mL GO scaffold (A–D) and control (E–H) implanted in rat subcutaneous tissue at 10 days and 1 µg/mL GO scaffold (I–L) and control (M–P) at 35 days. Infiltration of ED2-positive cells and ASMA-positive arterioles was more remarkable in the GO scaffold than in the collagen scaffold.

The bioactivity of GO scaffold

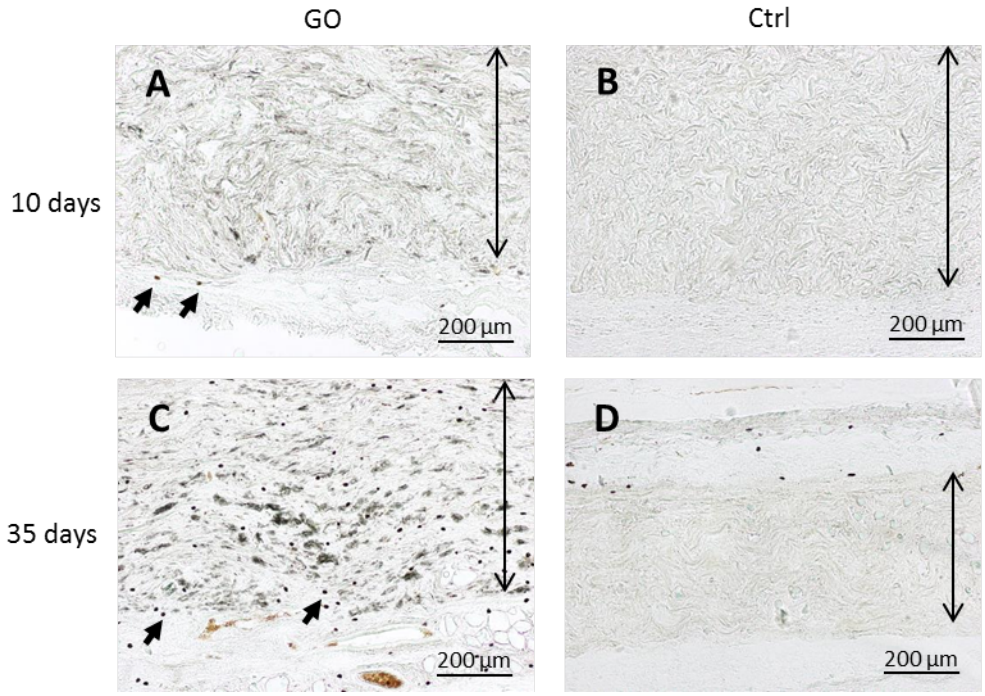

Figure 6

Peroxidase-stained activity for granulocytes in implanted 1 µg/mL GO scaffold (A) and control (B) in rat subcutaneous tissue at 10 days and 1 µg/mL GO scaffold (C) and control (D) at 35 days. Peroxidase-positive granulocytes (arrows) were detected slightly around GO scaffold. Double arrows indicate the implanted scaffold.

The bioactivity of GO scaffold

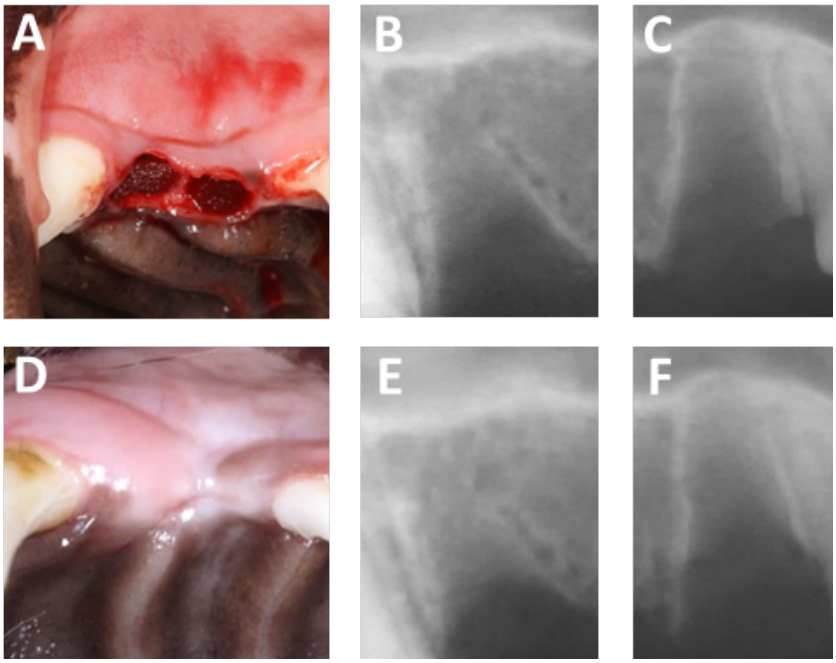

Figure 7

(A) Photograph of implanted scaffold. (B) Radiographic image immediately after operations for control (C) Radiographic image immediately after operations for 1μg/mL GO scaffold. (D) Macroscopic view at 2 weeks post-surgery. (E) Radiographic image at 2 weeks post-surgery for control. (F) Radiographic image at 2 weeks post-surgery for 1μg/mL GO scaffold.

The bioactivity of GO scaffold

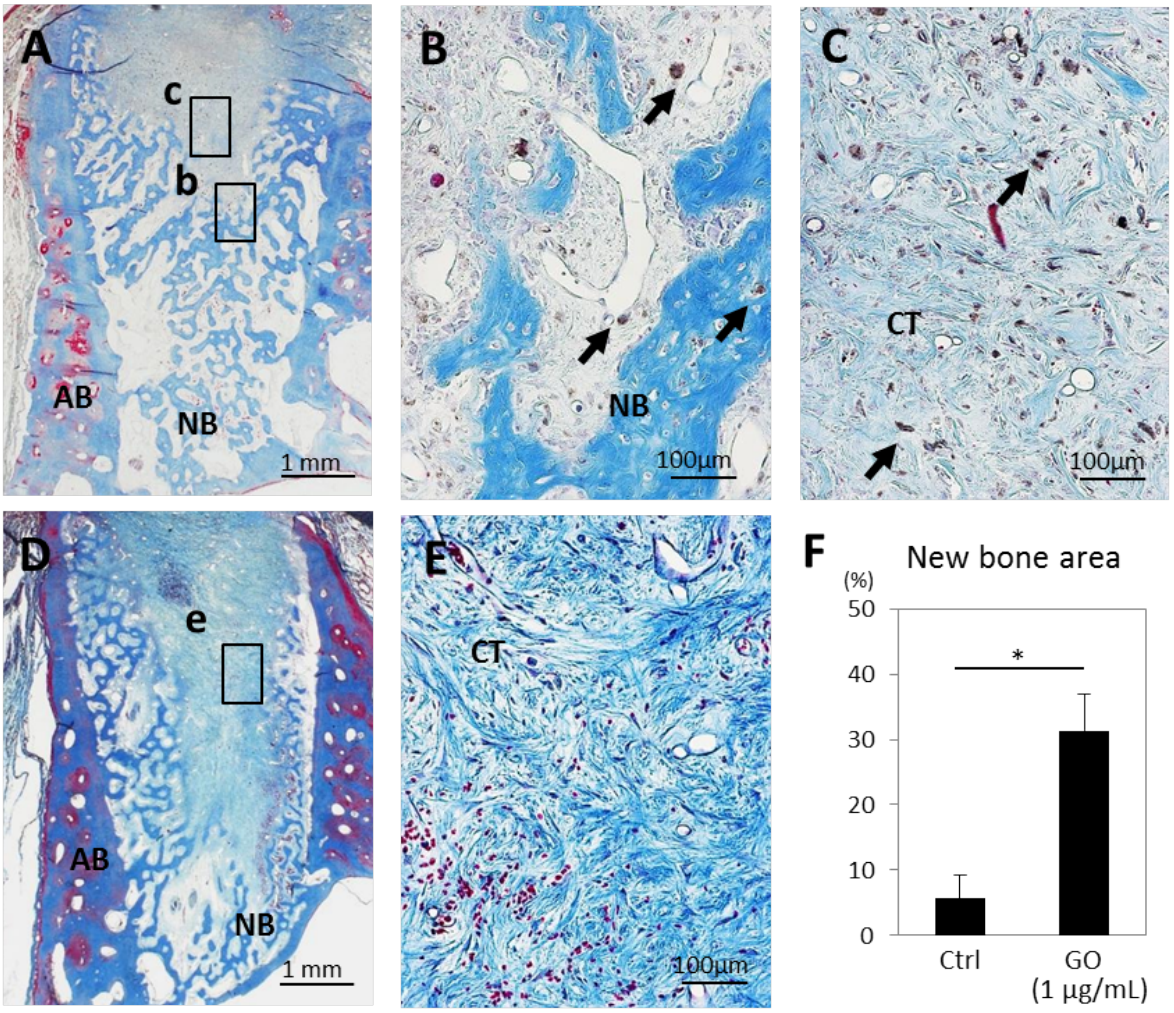

Figure 8

Histological findings in extraction socket at 2 weeks. (A) Specimen receiving 1 μg/mL GO scaffold. (B, C) Higher magnification of the framed area (b, c) in (A). Residual GO (arrows) were observed in newly formed bone and connective tissue. (D) Specimen receiving control material. (E) Higher magnification of the framed area (e) in (D). Masson's trichrome staining. Abbreviations: AB, alveolar bone; NB, new bone; CT, connective tissue. (F) Histomorphometric measurements of newly formed area. *: $P<0.05$.